Online ISSN: 2981-0396 Print ISSN: 2981-0388

International Journal of Iron & Steel Society of Iran

Journal Homepage: https://journal.issiran.com/

Research Article

Tribological Behavior of Weld Zone in TIG-Welded AISI410 Martensitic Stainless Steel

M. Rafiei *[1], H. Mostaan [2], A. R. Bakhshandeh [3], S. Ghaderi [4]

[1] *Advanced Materials Research Center, Department of Materials Engineering, Najafabad Branch, Islamic Azad University, Najafabad, Iran*
[2, 3, 4] *Department of Materials and Metallurgical Engineering, Faculty of Engineering, Arak University, Arak, Iran*

ARTICLE INFO

Keywords:

AISI 410, GTAW, Wear behavior, Hardness, Weld joint.

Article history:

Received 23 August 2024
Received in revised form 15 November 2024
Accepted 16 April 2025

ABSTRACT

The influence of different filler metals on tribological properties of TIG-welded AISI410 steel was studied. The microstructure and tribological properties of the welded samples were detected via optical microscopy, scanning electron microscopy and reciprocating wear test. Additionally, the hardness of the weld zone in different samples was measured via the Vickers hardness test. The microstructure of the welded sample with the ER80S filler metal with a Cr_{eq}/Ni_{eq} ratio of 1.6 was fully martensitic, whereas in the welded sample with the ERNiCrCoMo-1 filler metal with a Cr_{eq}/Ni_{eq} ratio of 0.66, only an austenitic microstructure was observed. Additionally, the welded sample with an ER410 filler metal Cr_{eq}/Ni_{eq} ratio of 3.1 had a dual-phase microstructure containing ferrite grains and tempered martensite; in contrast, the welded sample with an ER312 filler metal with Cr_{eq}/Ni_{eq} ratio of 2.35 had a dual-phase microstructure containing columnar austenite and interdendritic and vermicular ferrite. Compared with the other weld metals, the sample welded with the ER80S filler metal had a greater hardness (560 HV) and therefore lower mass loss (40 mg) owing to the formation of a fully martensitic microstructure. The wear mechanism of the samples welded with ER80S and ER410 filler metals was delamination, whereas in the samples welded with ERNiCrCoMo-1 and ER312 filler metals, microplowing abrasives and abrasive and adhesive wear mechanisms were seen, respectively.

1. Introduction

In recent years, martensitic stainless steels (MSSs) have been widely used for different industrial applications owing to their excellent properties, such as good corrosion behavior, high toughness at low temperatures, and high rate of work hardening. Martensitic stainless steels have at least 13% Cr and have high strength and hardness. Moreover, owing to their high hardenability, a prolonged cooling rate is sufficient to obtain a martensitic microstructure [1–4]. They can be used in turbines, valves and different parts of aircraft, pressure vessels, cutlery, piping, oil, and power plant industries. These alloys are used in thermal generators owing to their high-temperature strength [5]. Owing to the good performance of these alloys under corrosive conditions and their high

* *Corresponding Author*
Email: m.rafiei@iau.ac.ir
Address: Advanced Materials Research Center, Department of Materials Engineering, Najafabad Branch, Islamic Azad University, Najafabad, Iran
1. Associate Professor, 2. Associate Professor, 3. M.S., 4. M.S.

DOI: http://10.22034/IJISSI.2025.2039415.1302
Published by ISSI (Iron & Steel Society of Iran)

resistance to thermal and mechanical shocks, these steels are good choices for producing turbine blades and internal parts of industrial valves [6]. Because of their high strength in addition to their corrosion resistance, martensitic stainless steels are also good candidates for materials subjected to both corrosion and wear [7–9]. MSSs are the cheapest grade of stainless steels owing to the low percentage of alloying elements. MSSs have high hardenability, and their microstructure mostly contains the martensite phase. However, because of the high yield strength and low ductility of the martensite phase, these steels are usually produced with ferritic microstructure. After forming or welding, their microstructure becomes martensite after heat treatment [10–12].

One of the most important MSSs is AISI410, with more than 0.12 wt.% carbon [13]. This steel is widely used in various industrial applications, including the construction, automotive, aerospace, and food and medical industries. The combination of corrosion resistance, strength, and hardness makes it an excellent choice for a wide range of applications. The major weakness of this steel is its poor weldability, and this steel is susceptible to hydrogen-induced cracking [13]. Fusion welding of this type of steel is challenging, as this material is highly vulnerable to hot and cold cracking. Additionally, the formation of the martensite phase and hydrogen embrittlement are critical [14].

Wear is a significant degradation mechanism of materials whose relative movements differ. The detection of the primary wear mechanism in materials can help to avoid abrupt failure. The main wear mechanisms are abrasive, adhesive, delamination, and oxidation, which occur according to tribosystem conditions and affect the wear rate and friction coefficient. The formation of an oxidation layer with low shear strength can decrease the friction coefficient and therefore decrease the wear rate. These oxidation layers, in addition to creating wear particles during the wear process, can affect wear and friction and change the predominant wear mechanism. The selection of the best way to control the wear rate is vital in industry. Several methods, such as coating, cladding, hard-facing, changing surface chemistry by different coatings, and welding methods, are used to create wear-resistant surfaces. In welding, the selection of a suitable filler metal or electrode is of prime importance to create a wear-resistant surface. Several studies have investigated these methods to control the wear rate of materials [15–18]. In fusion welding, because different solidified microstructures are created, the wear behavior of the welded zone is complicated and needs to be studied further. Therefore, the study of the wear behavior of the weld zone is essential for postponing material deterioration. As reported previously [19-21], different phases, due to their different properties, indicate different wear rates. In the fusion welding process, owing to the formation of different microstructures in the weld and heat-affected zones (HAZs), the wear rate of the weld affects the created microstructures. The subzones of a weld metal with different microstructures have different wear rates and frictional forces because of the variation in hardness values. Wang et al. [20] reported that the microstructure significantly influences the wear resistance of a given material. The effect of the microstructure on the wear rate of a material depends on its stability with respect to frictional heating, resistance to plastic deformation, and resistance to the initiation and propagation of microcracks [21].

There are several studies on the fusion welding of martensitic stainless steels in the literature [22, 23]. Hejripour and Aidun [24] studied the fusion welding of 410 stainless steel to Inconel 718. They reported that the hardness in the HAZ of 410 steel is greater than that in the weld zone and 410 base metal because of the formation of the hard martensite phase. The area adjacent to the fusion boundary in the HAZ included the ferrite and martensite phases. The soft ferritic region was observed in this zone. The area further from the fusion boundary had a completely martensitic structure. Puli and Janaki Ram [14] investigated the wear performance of an AISI410 steel coating. They reported that manual metal arc coatings had lower hardness and wear resistance as compared with the produced coatings with friction surfacing because of the formation of δ-ferrite during solidification. Casalino et al. [25] studied the weldability of 304 to 410 stainless steels via laser/TIG hybrid welding. They reported that in the HAZ of 410 martensitic stainless steel, the grain boundaries of the ferrite phase contained a continuous martensite layer that had formed at elevated temperatures.

There are very few studies on the wear behavior of weld zone in fusion welding. Additionally, no research in the scientific literature has investigated the wear behavior of the weld zone in AISI410 steel with changes in the chemical composition of the weld zone. Therefore, in this work, for the first time, the effects of different microstructures induced by different filler metals on the wear behavior of the weld zone in GTAW welded AISI410 steel were investigated. For this purpose, different filler metals were used for welding, and the effects of the formed microstructures on the degree of wear were studied.

2. Materials and Methods

In this research, an AISI410 martensitic stainless steel plate was used as the base material. Additionally, four different filler metals, including ER410, ER80S-B2, ERNiCrCoMo-1, and ER312 with a diameter of 1.8 mm, were used for the welding process. Table 1. presents the chemical compositions of the base, filler, and weld metals. These filler metals were selected according to Fig. 2. and on the basis of different Cr_{eq}/Ni_{eq} ratios.

The gas tungsten arc welding (GTAW) process was used for welding the plates. The dimensions of the samples and the weld design used are presented in Fig. 1.

The welding process was performed in four passes without preheating, with an interpass temperature of approximately 50 °C. The current, voltage, and speed of the welding process were 140 A, 15 V, and 1.5 mm.s^{-1}, respectively. Additionally, the process was carried out with a W-2%ThO_2 electrode under pure Ar protective gas with a flow rate of 10 L.min^{-1}. DCEN polarity was used for the welding. Meanwhile, for all filler metals and welding passes, the same parameters were used. The peak temperature, heat input, HAZ width, and cooling rate of the welding process were calculated via the following formulas and data from Table 2. [13, 26].

$$\frac{1}{T_P - T_0} = \frac{4.13 V y g \rho C_P}{Q} + \frac{1}{T_m - T_0} \quad \text{Eq.(1)}$$

$$Q = \frac{\eta V I}{\upsilon} \quad \text{Eq.(2)}$$

$$R = 2\pi K \rho C_P \left(\frac{g}{Q}\right)^2 (T_i - T_0) \quad \text{Eq.(3)}$$

Table 1. Chemical compositions of the base, filler and weld metals.

	Alloy	Chemical composition (wt.%)											
		C	Mn	Si	Ni	Cr	Mo	S	P	Cu	Fe	Co	Al
Base metal	AISI410	0.12	1	1	0.75	13.5	0.5	0.03	0.04	---	Balance	---	---
Filler metal	ER410	0.12	0.55	0.5	0.5	12	0.65	0.03	0.03	0.65	Balance	---	---
	ER80S-B2	0.1	0.7	0.1	---	1.3	0.55	0.025	0.025	0.35	Balance	---	---
	ERNiCrCoMo-1	0.1	0.7	0.95	Balance	22.5	8.55	0.01	0.03	0.45	2.5	11.5	0.88
	ER312	0.1	1.7	0.55	10.33	29.5	0.7	0.03	0.03	0.55	Balance	---	---
Weld metal	ER410	0.12	0.68	0.65	0.57	12.45	0.6	0.03	0.033	0.45	Balance	---	---
	ER80S-B2	0.1	0.8	0.37	0.22	4.96	0.53	0.026	0.029	0.24	Balance	---	---
	ERNiCrCoMo-1	0.1	0.79	0.96	Balance	19.8	6.13	0.01	0.02	0.31	26.05	8	---
	ER312	0.1	1.5	0.68	7.45	24.7	0.64	0.03	0.033	0.38	Balance	---	---

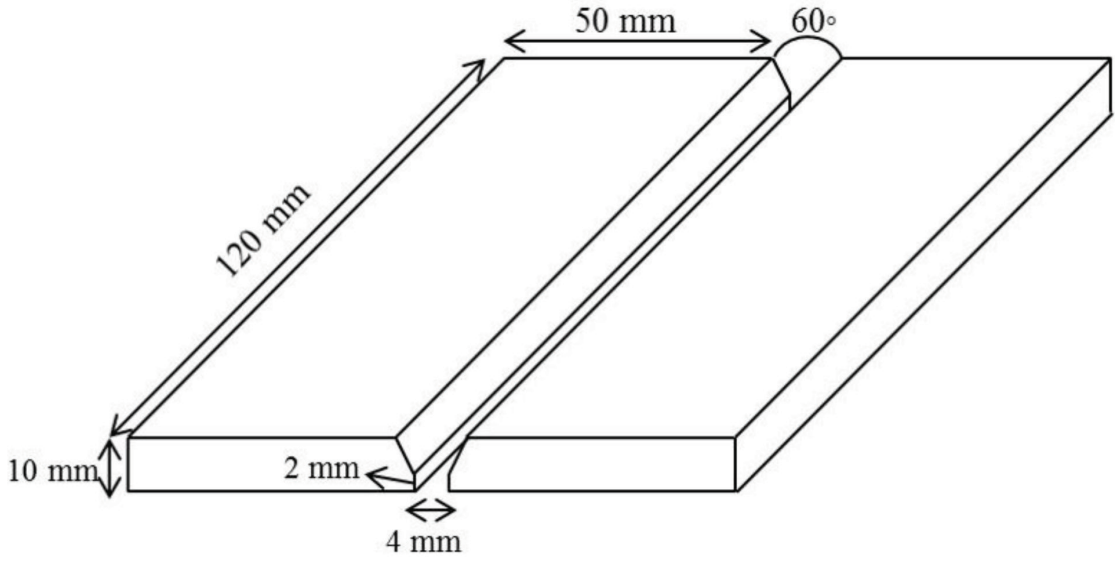

Fig. 1. Dimensions of the plates and the used weld design.

In Eq.(1), T_p is the peak temperature, T_0 is the initial temperature, υ is the welding speed, y is the distance from the fusion line, g is the material thickness, ρ is the density, C_p is the specific heat capacity, T_m is the melting point of the material, and Q is the heat input.

In Eq.(2), η is the efficiency, V is the welding voltage, I is the welding current, and in Eq.(3), R is the cooling rate, K is the thermal conductivity, and T_i is the temperature of interest.

For metallography, some samples were cut from the plates and prepared via conventional mechanical polishing methods. The samples were prepared by grinding using P120–P2000 grit silicon carbide paper according to the FEPA standard and polished with a 0.3 μm alumina solution. The samples were etched with the various solutions listed in Table 3.

The microstructures of the welded samples at different areas, including the base metal, HAZ, and weld metal, were observed via an IM 420 optical microscope (OM). The chemical compositions of the welded samples were obtained via optical emission spectroscopy (OES) with the Foundry–Master PRO model.

The hardness of the weld zone in different samples was measured via the Vickers hardness test method under a load of 200 g and dwell time of 10 s. The tribological properties of the weld zone in different welded samples were evaluated by reciprocating wear test. The samples were washed with detergent and water to remove any residual oils or talc and then dried at 150 °C before the test. This wear test was chosen because of the special geometry of the welded samples (rectangular shape). A reciprocating wear test was performed via a TE 38 long-stroke low-load reciprocating tribometer (made in China) on the surface (top) of the welded samples through the weld bead using an AISI 52100 ball with a hardness of 65 HRC and a microstructure consisting of tempered martensite with homogeneously distributed $(Fe,Cr)_3C$ carbides and approximately 10–12% retained austenite with a diameter of 9 mm at an ambient temperature and a humidity of 30%. The 52100 tool steel is a cold, high-carbon chromium steel with suitable wear resistance that is usually used as a ball in wear tests. The sliding distance, mean sliding speed, stroke length, and normal load were 1000 m, 0.1 $m.s^{-1}$, 10 mm, and 50 N (dead weight), respectively. The ASTM G133 standard was used for sample preparation before the test. On average, three tests were performed for each condition. The mass losses of the samples after the wear test were measured via an accurate balance and compared by generating a mass loss versus filler metal graph. Finally, the wear tracks of different samples were observed by scanning electron microscopy (SEM) in an LEO 435VP instrument equipped with an energy dispersive spectrometer (EDS) analyzer using both secondary and backscattered electrons (SE and BSE) to clarify the wear mechanism.

3. Results and Discussion

3.1. Prediction of the Weld Structure Via the Schaeffler Diagram

A Schaeffler diagram was used to predict the solidified microstructures of the weld metals with different filler metals, as shown in Fig. 2. For this purpose, the dilution of the welding process was calculated to be approximately 30%. Additionally, Eqs.(4) and (5) were used for calculating the

Table 2. Physical properties of the AISI410 steel used in the calculations.

T_m (°C)	T_0 (°C)	ρ ($g.cm^{-3}$)	K ($W.cm^{-1}.°C^{-1}$)	C_P ($J.g^{-1}.°C^{-1}$)
1530	50	7.8	0.25	0.46

Table 3. Chemical composition of the etchants used in this study.

Filler Metal	Composition	Etching time (s)
ER 410	1.5 g $CuCl_2$, 33 ml HCl, 33 ml ethanol, 33 ml H_2O (Kalling)	15
ER 312	Equal parts HCl, HNO_3, and acetic acids (Mixed acids)	30
ER NiCrCoMo-1	15 ml glycerol, 10 ml HCl, and 5 ml HNO_3 (Glyceregia)	15
ER 80S-B2	5 ml HNO_3 in 100 ml of ethanol (Nital)	10

Ni_{eq} and Cr_{eq} values, respectively.

$$Ni_{eq} = \%Ni + 30\%C + 0.5\%Mn \quad \text{Eq.(4)}$$

$$Cr_{eq} = \%Cr + \%Mo + 1.5\%Si + 0.5\%Nb \quad \text{Eq.(5)}$$

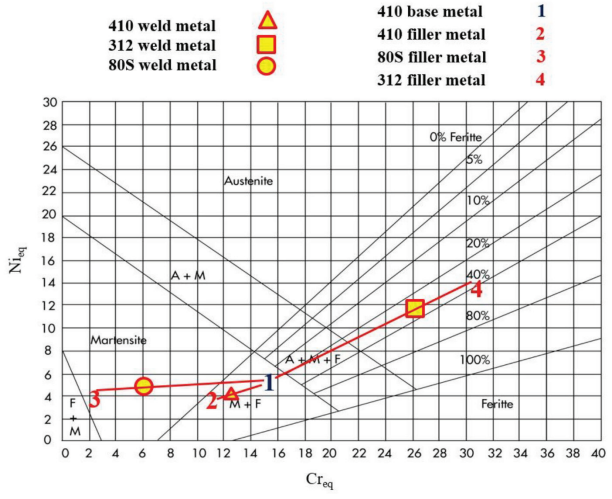

Fig. 2. Positions of different bases, fillers and weld metals on the Schaeffler diagram.

As seen in the ER410 weld metal, the Schaeffler diagram predicts that the microstructure of the weld metal is composed of martensite and ferrite phases. The value of Cr_{eq}/Ni_{eq} in this weld metal is equal to 3.1. The high value of this ratio shows that the austenite phase is not stable in the weld metal after solidification. The lack of an austenite phase and the presence of a brittle martensite phase increase the possibility of crack formation during cooling. However, the presence of the ferrite phase seems natural regarding a high amount of ferrite former elements in this weld metal.

The ferrite phase can decrease the possibility of crack formation and increase the toughness of the weld metal. However, for the ER80S weld metal with a Cr_{eq}/Ni_{eq} ratio of 1.6, a fully martensitic microstructure is observed. Compared with that of the ER410 weld metal, the content of former ferrite elements is lower, and a lack of the ferrite phase is expected. This weld metal is susceptible to cracking and has a low toughness compared with previous weld metal. The formation of this weld metal creates challenging conditions for impact tolerance. The formation of a fully martensitic structure is reasonable regarding the chemical composition of this weld metal (Table 1.).

According to the Schaeffler diagram, a fully austenitic microstructure is created in the ERNiCrCoMo-1 weld metal owing to the high content of Ni in the filler metal. Ni-based filler metals have been used as preferred filler metals for the welding of brittle materials such as cast irons, Ni-based alloys, and stainless steels [27, 28]. The location of this weld metal is not specified in the Schaeffler diagram because of the high Ni_{eq} (approximately 40), which is out of the diagram. Although the formation of this microstructure increases the ductility of the weld metal, it can be susceptible to hot cracking because of the lack of a ferrite phase. On the basis of the Cr_{eq}/Ni_{eq} ratio of this weld metal, which is equal to 0.66, the high value of former austenite elements encourages the formation of the austenite phase. Eventually, for the ER312 weld metal with a Cr_{eq}/Ni_{eq} ratio of 2.35, an austenite/ferrite dual-phase microstructure formed. This structure, with a suitable toughness, can prevent the formation of hot cracks owing to the presence of the ferrite phase.

3.2. The Microstructure of The Fusion Boundary and HAZ

According to the calculations via Eqs.(1) and (2), the HAZ width was calculated to be approximately 6 mm. For this purpose, the distance from the fusion boundary to a peak temperature of 723 °C was calculated. Fig. 3. shows the fusion boundary and coarse grain HAZ in different welded samples with different filler metals.

According to Fig. 3(a). grain growth is observed in the HAZ of the sample welded with the ER80S filler metal. In this zone, coarse grains of ferrite with some martensite phase at the grain boundaries are observed. This coarse grain zone and the presence of martensite in the grain boundaries can decrease the strength and toughness and increase the susceptibility to cracking in this zone, which leads to failure under tension stress. By moving away from the fusion boundary to the HAZ/base metal interface and decreasing the peak temperature from 1530 to 723 °C, a finer microstructure of ferrite grains and tempered martensite with better mechanical properties, such as strength and toughness, is observed. This figure shows that in the fusion line, nearly epitaxial growth is observed owing to the similarity of the chemical compositions of the base and weld metals, according to Table 1. The formation of this structure in the fusion line decreases the mechanical stress gradient in this zone and results in homogenous mechanical properties.

According to Fig. 3(b). ferrite grains and grain boundary martensite were observed in the HAZ of the welded sample with the ERNiCrCoMo-1 filler metal, whereas the structure of the weld metal was not visible. For the ER410 weld metal, a similar structure was observed in the HAZ. For this sample, the width of the coarse-grained HAZ and the grain growth of this zone were lower than those of the welded sample with the ER80S filler metal. This is due to the chemical composition effect of the weld metal on heat transfer and, eventually, its impact on grain growth and the width of the coarse-grain HAZ. In this image, the structure of the weld metal and the fusion line are not recognizable. Finally, in the sample welded with the ER312 filler metal, the coarse-grained microstructure of the HAZ consists of coarse ferrite grains, and the martensite phase is observed. By moving toward the base metal, the ferrite and tempered martensite phases were seen. It can be said that owing to the welding heat input, the martensite phase has been tempered. In this welded sample, the nucleation of new grains with

different orientations by the grains of the base metal was observed, indicating nonepitaxial growth during solidification of the weld pool. This growth mode of the weld metal is due to the different structures of the weld and base metals. The weld metal of this sample contains ferrite and austenite phases, whereas the base metal contains ferrite and martensite phases.

3.3. Microstructures of the Weld Metals

Fig. 4. shows the microstructures of the different weld metals. As shown in Fig. 4 (a). the microstructure of the sample welded with the ER80S filler metal is fully martensitic, which is in good agreement with the prediction of the Schaeffler diagram.

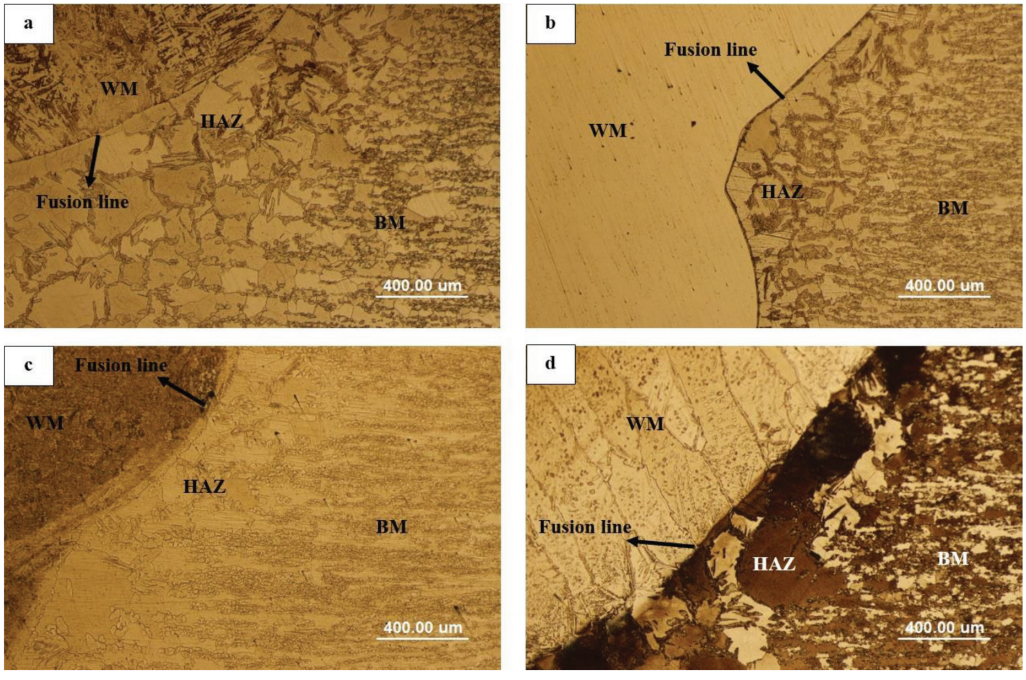

Fig. 3. Optical microscope images indicating the weld metal, HAZ and base metal for the welded samples using (a) ER80S, (b) ERNiCrCoMo-1, (c) ER410 and (d) ER312 filler metals.

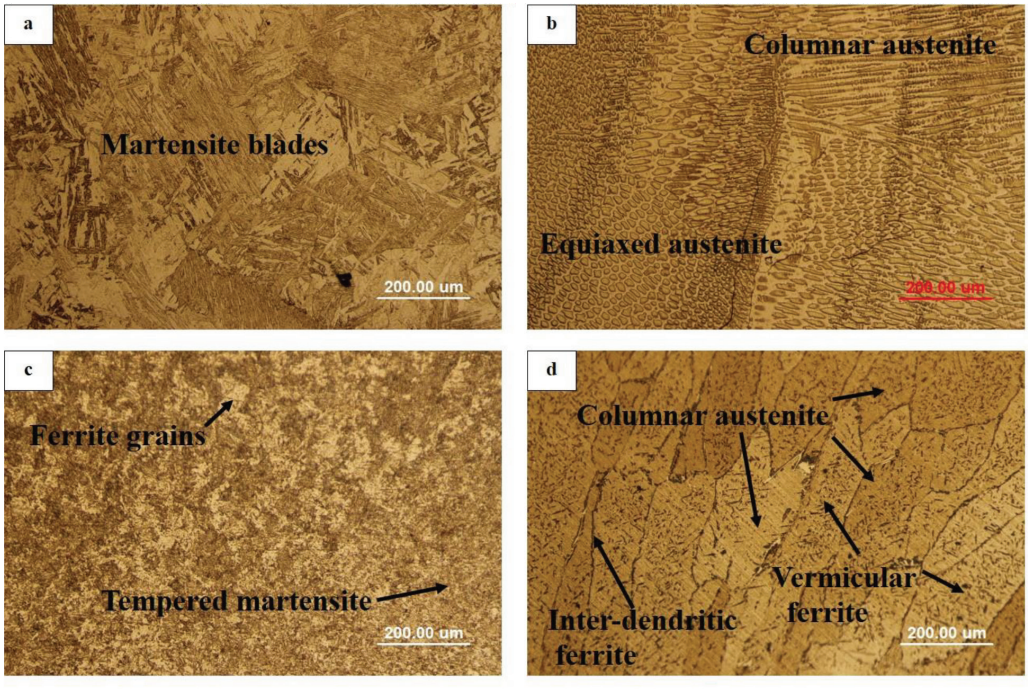

Fig. 4. Optical microscope images indicating the weld metals of the welded samples using (a) ER80S, (b) ERNiCrCoMo-1, (c) ER410 and (d) ER312 filler metals.

This image indicates a fully shear structure with a coarse lath in the martensite phase. This structure has been formed owing to the chemical composition of the weld metal (Table 1.) and the high cooling rate (approximately 1.21 °C.s^{-1} from 800 to 500 °C, which was calculated via Eq.(3) of the weld metal after welding. Martensite, which acts as a hard domain, is susceptible to crack initiation and growth and plays a significant role in enhancing strain-hardening ability and achieving large uniform elongation due to its high stress-increasing potential. However, the presence of hard martensite also imposes restrictions on post-uniform elongation due to the strong strain localization induced in the microstructure. In the welded sample, when ERNiCrCoMo-1 filler metal was used, a fully austenitic microstructure consisting of fine columnar and equiaxed dendrites was observed. Compared with the martensite phase, this phase has a lower hardness and strength, greater toughness and a lower possibility of crack formation. The Schaeffler diagram also predicted this microstructure. According to Fig. 4(c). the welded sample with the ER410 filler metal exhibited a dual-phase microstructure containing ferrite grains and tempered martensite, which is similar to the typical microstructure of AISI410 steel.

Fig. 4(d). shows the microstructure of the sample welded with the ER312 filler metal. A dual-phase microstructure contains columnar austenite and interdendritic material, and vermicular ferrite is observed in this weld metal. This microstructure can prevent the formation of hot cracks during the solidification of the weld metal. Moreover, this structure has a good combination of toughness and strength. All the microstructures observed in the different welded samples were well predicted by the Schaeffler diagram.

3.4. Tribological Properties of the Weld Metals

Fig. 5. shows the bar diagram of mass loss after the wear test for the welded samples. The welded sample with the ER80S filler metal had the lowest mass loss after 1000 m of sliding distance. It can be concluded that the welded sample with the ER80S filler metal has the best wear resistance compared with the other welded samples. As previously mentioned, the weld metal of this sample had a fully martensitic microstructure (Fig. 4.) with a microhardness value of approximately 560 HV. The presence of this structure with high hardness is one of the most important factors responsible for the high hardness and higher wear resistance of this sample compared with those of the other welded samples. The martensite phase is a supersaturated solid solution of carbon in ferrite with a body-centered tetragonal (BCT) crystal structure. During rapid solidification, carbon is trapped in the crystal structure. The hardness increases as a result of the distortion that occurs during the transformation from FCC austenite to BCT martensite and the fine dislocation substructure that develops in the martensite crystals during the diffusionless shear transformation. Additionally, strain hardening of worn surfaces during wear tests usually results in a much greater hardness under steady-state conditions. After this sample, the ER410 weld metal showed the lowest mass loss after the wear test. In this sample, as previously mentioned, the presence of tempered martensite and ferrite phases led to greater wear resistance than in the sample welded with the ER312 filler metal (with a hardness of 265 HV), but it displayed lower wear resistance compared to the sample welded with the ER80S filler metal owing to its microstructure (tempered martensite and ferrite with lower distortion and hardness than the fully martensite microstructure). In fact, the tempering of the martensite phase decreases the residual stresses and hardness of this phase. The weld metal of the sample welded with the ER312 filler metal (with a hardness of 265 HV) had weak wear resistance compared with that of the samples welded with the ER80S and ER410 filler metals. This is because of its microstructure (austenite + ferrite) and the lack of martensite phase in this weld metal. Compared with the ERNiCrCoMo-1 filler metal, the presence of a ferrite phase in this weld metal, which creates a composite microstructure, increased the hardness. Finally, the sample welded with the ERNiCrCoMo-1 filler metal experienced the greatest mass loss (approximately 120 mg) after the wear test, indicating that it had the lowest wear resistance compared with the other welded samples because of its ductile austenite single-phase microstructure (with a hardness of 230 HV).

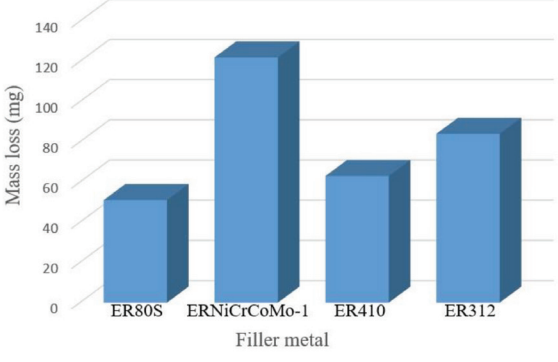

Fig. 5. Mass loss of different weld metals after the wear test.

Fig. 6. shows SEM images of the wear tracks of the samples welded with different filler metals. As shown in Fig. 6(a, b). several branched cracks are observed in the wear track of the sample welded with the ER80S filler metal, indicating a delamination wear mechanism.

According to Fig. 4(a). the welded sample with this filler metal had a fully martensitic microstructure with a hardness of 560 HV. However, the presence of this hard structure provides excellent wear resistance, but owing to the high tension and distortion in this structure and its brittle nature, the occurrence of a delamination wear mechanism is probable. In this wear mechanism, the

accumulation of dislocations near the surface (martensite blades) leads to the formation and linking of voids and the formation of subsurface cracks. This process leads to the creation of delaminated particles from the surface. In Suh theory [29], the pile-up of dislocations and the work hardening of the material near the surface results in void and crack formation in this zone. In this theory, cracks and voids can join together via three mechanisms: void growth, crack propagation, and plastic shear deformation of the material between the voids. In this sample, owing to the presence of the martensite phase and its brittle nature, it seems that the crack propagation mechanism is governed. In this mechanism, the wear particles do not create until other cracks nucleate. In this state, owing to the very low plastic shear deformation of the surface, a high number of cracks must be created before the formation of wear particles. The formation of several branched cracks in the wear track of this sample is shown in Fig. 6(a, b). Finally, the creation of these cracks leads to the formation of delaminated particles. Additionally, when the material is brittle, the delaminated wear particles are broken into several smaller particles [29]. According to Fig. 8(a). this sample has an average friction coefficient of approximately 0.6 owing to its low plastic deformation and high hardness. Additionally, the high oscillation of the friction coefficient can be attributed to several factors, including the formation of delaminated wear particles and the shredding of particles between worn surfaces, surface topography, stick–slip phenomena, tribometer dynamics, etc., which can change the friction coefficient value over a wide range. For example, the formation of delaminated wear particles can increase or decrease the friction coefficient. If these particles are spherical, can increase the degree of slip and therefore decrease the friction coefficient, whereas nonspherical particles increase the degree of slip difficulty by increasing mechanical interlocking. Additionally, surface topography parameters such as the arithmetic mean height amplitude, surface height distribution kurtosis, surface volume average volume, and surface center area average void volume can affect the friction coefficient differently.

For the sample welded with the ERNiCrCoMo-1 filler metal (Fig. 6(c, d).), the wear track reveals parallel grooves beside the depressed areas induced by plastic deformation of the surface and indicates an abrasive wear mechanism. As shown in Fig. 4(b). the weld metal of this sample had a ductile fully austenitic microstructure with a low hardness of approximately 230 HV. The wear surface confirms the occurrence of plastic deformation. Under this wear condition, displacement of the material from the groove toward the edges occurs and finally leads to the formation of wear particles because of the work hardening effect. In fact, in this sample, the microplowing mechanism creates several grooves on the surface of the material. Wang et al. [20] reported that the microstructure significantly influences the wear resistance of a given material. The effect of the microstructure on the wear rate of a material depends on its stability with respect to frictional heating, resistance to plastic deformation, and resistance to the initiation and propagation of microcracks [21]. As shown in Fig. 8(b). owing to the occurrence of this wear mechanism, a relatively high average friction coefficient of approximately one was observed compared with that of the other samples. The force needed for plastic deformation and the plowing effect increased the friction coefficient.

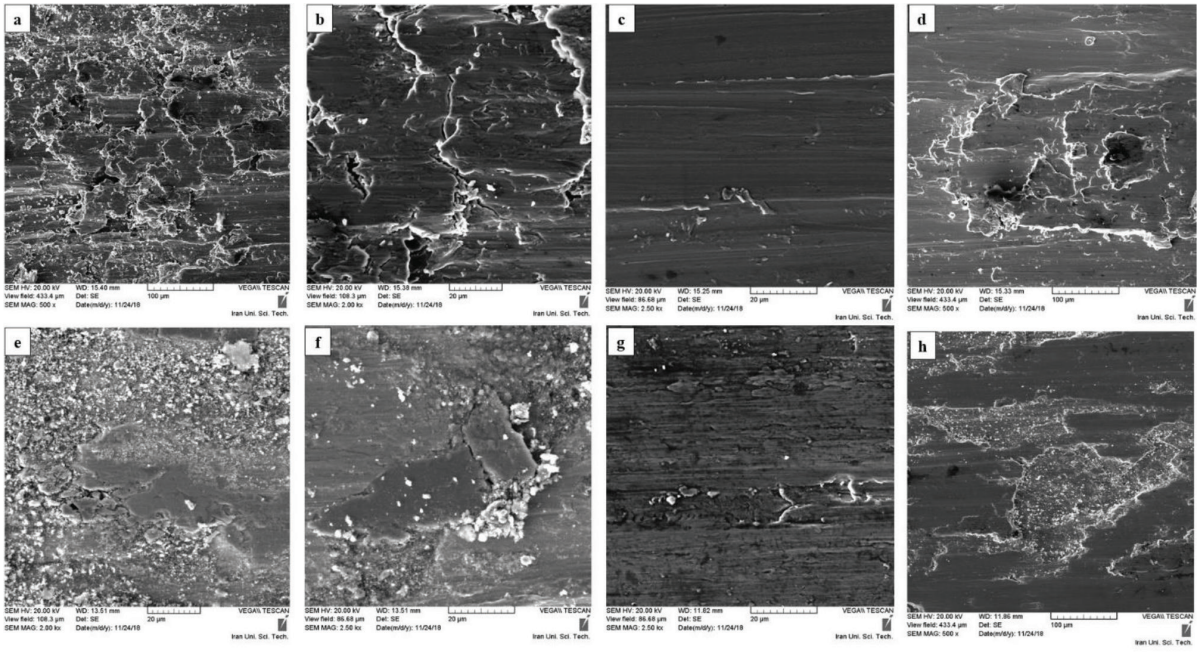

Fig. 6. SEM images of the wear tracks of the samples welded with (a, b) ER80S, (c, d) ERNiCrCoMo-1, (e, f) ER410 and (g, h) ER312 filler metals.

For the sample welded with the ER410 filler metal, delamination wear is the predominant mechanism of wear, which can be observed with crack formation on the wear track (Fig. 5 (e, f)). The microstructure and hardness of this welded sample (Fig. 4(c).) indicate that the plastic deformation of the surface is greater than that of the sample welded with the ER80S filler metal, which indicates a fully martensitic microstructure. It can be concluded that void growth can lead to crack propagation. Moreover, according to Fig. 7(b). on the wear surface of this sample, the presence of oxygen was observed, indicating an oxidation wear mechanism and the formation of oxide islands. The presence of these oxide compounds on the surface of this sample with low shear strength can decrease the mean friction coefficient (Fig. 8(c).) Fig. 6(g, h). shows the wear track of the sample welded with the ER312 filler metal. Several thin grooves and signs of material removal demonstrated the occurrence of both abrasive and adhesive wear mechanisms. With respect to the activation of these wear mechanisms, the friction coefficient of this sample is expected to be high, but according to Fig. 8(d). the lowest mean friction coefficient was observed for this sample. This occurred because of the formation of oxide islands in the wear track, according to the EDS analysis presented in Fig. 7(a). As previously mentioned, the presence of oxide islands can decrease the friction coefficient of the surface. Additionally, the formation of these oxide islands can lead to the easier removal of adhesive wear particles during the wear test. In fact, in this state, the shear strength of the connecting area is greater than that of farther areas, and failure occurs from the worn material and leads to an adhesive wear mechanism.

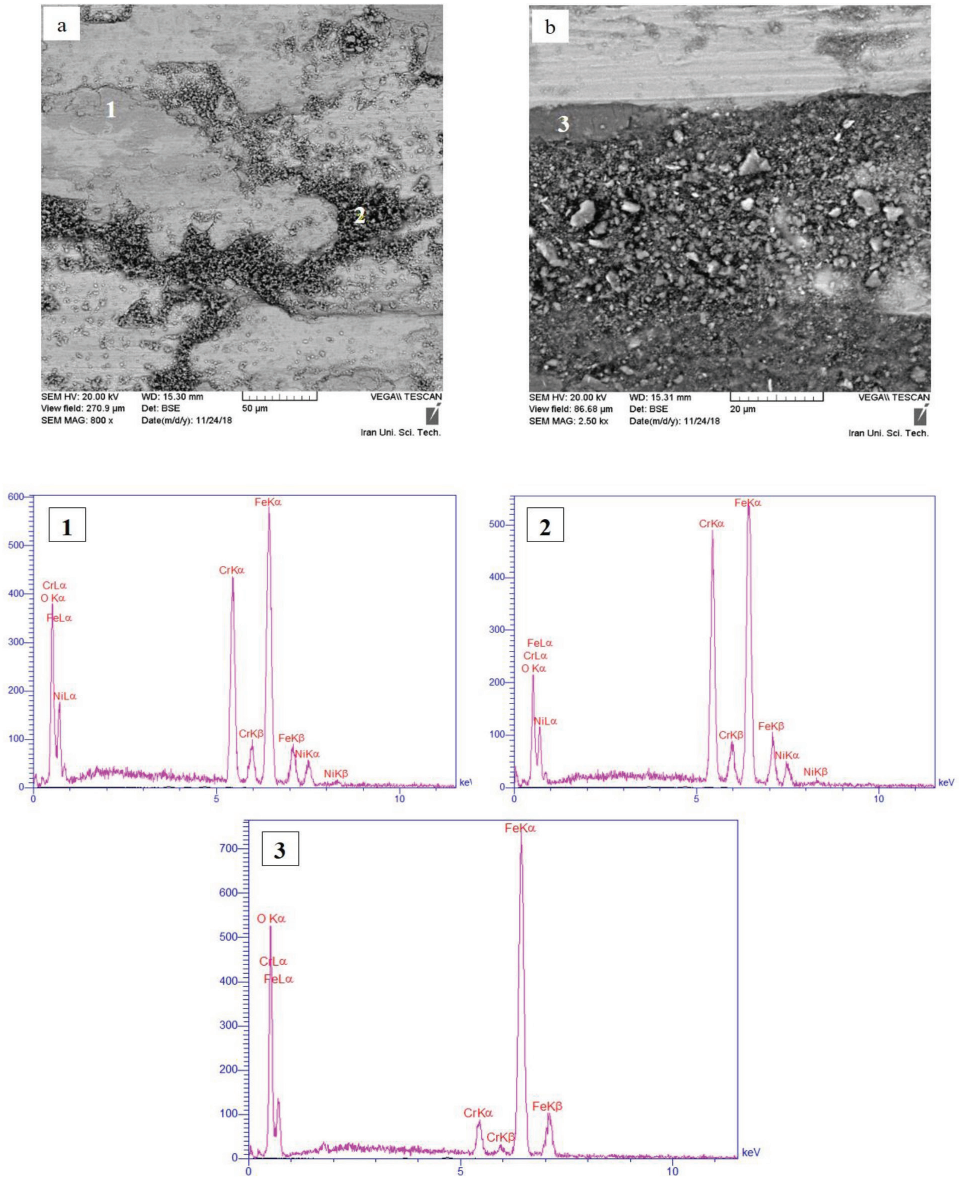

Fig. 7. SEM images from the wear track of the welded samples using (a) ER312 and (b) ER410 filler metals and corresponding EDS spectra.

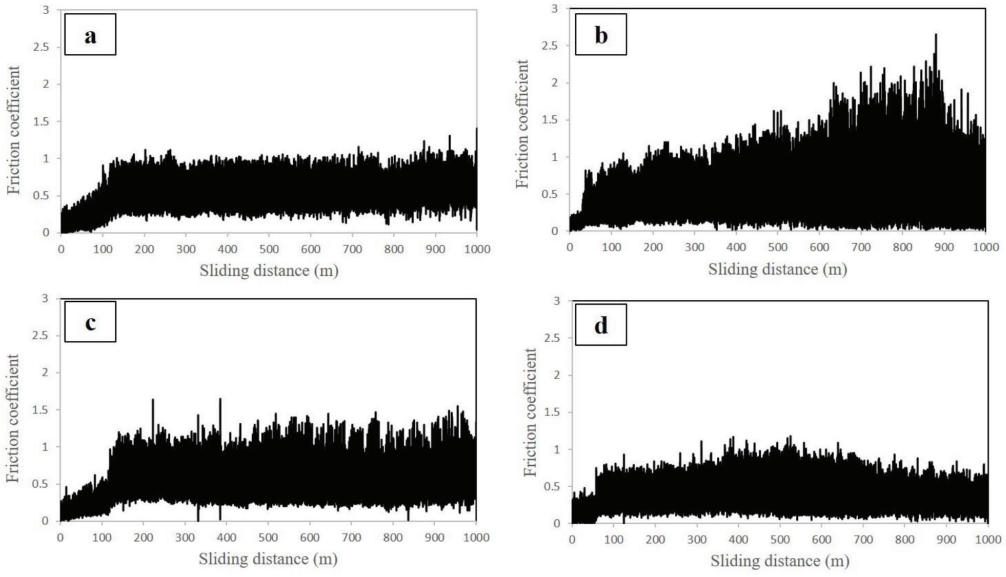

Fig. 8. Friction coefficient versus sliding distance during the wear test of the welded samples with (a) ER80S, (b) ERNiCrCoMo-1, (c) ER410 and (d) ER312 filler metals.

4. Conclusions

In this study, the effects of the chemical composition of the weld metal on the microstructure and tribological properties of welded AISI410 steel were investigated. For this purpose, four different filler metals were used for the welding process, and the following results were obtained:

- Grain growth was observed in the HAZ of the welded samples. In this zone, coarse grains of ferrite with some martensite phase were observed.
- The sample welded with the ER80S filler metal had a fully martensitic microstructure. In the sample welded with the ERNiCrCoMo-1 filler metal, a fully austenitic microstructure consisting of fine columnar and equiaxed dendrites was observed.
- The welded sample with the ER410 filler metal exhibited a dual-phase microstructure containing ferrite grains and tempered martensite, which is similar to the typical microstructure of AISI410 steel. The welded sample with the ER312 filler metal had a dual-phase microstructure containing columnar austenite and interdendritic and vermicular ferrite.
- The sample welded with the ER80S filler metal had the lowest mass loss during the wear test. This indicates that this sample has the best wear resistance compared with the other welded samples owing to its fully martensitic microstructure.
- The wear mechanism of the welded samples using ER80S, and ER410 filler metals was delamination, while in the welded samples using ERNiCrCoMo-1, and ER312 filler metals, microplowing abrasive, and abrasive and adhesive wear mechanisms, were seen, respectively. Additionally, in the welded samples using ER312 and ER410 filler metals oxidation wear mechanism was seen beside the mentioned mechanisms.

References

[1] Pouranvari M, Marashi S.P.H, Critical review of automotive steels spot welding: process, structure and properties. Science and Technology of Welding and Joining, 2013; 18(5): 361–403.

[2] Sun X, Stephens E.V, Khaleel M.A, Effects of fusion zone size and failure mode on peak load and energy absorption of advanced high-strength steel spot welds, Welding Journal (Miami, Fla). 2007; 86(1).

[3] Pouranvari M, Marashi S.P.H, Mousavizadeh S.M, Failure mode transition and mechanical properties of similar and dissimilar resistance spot welds of DP600 and low carbon steels, Science and Technology of Welding and Joining. 2010; 15(7): 625–31.

[4] Pouranvari M, Fracture toughness of martensitic stainless steel resistance spot welds, Materials Science and Engineering: A. 2017; 680: 97–107.

[5] Jafari M, Rafiei M, Mostaan H, Effect of Solidification Mode on Microstructure and Mechanical Properties of AISI420 Steel to SAF2507 Steel Dissimilar Joint Produced by Transient Liquid Phase, Metals and Materials International. 2019.

[6] Xi Y tao, Liu D xin, Han D, Improvement of corrosion and wear resistances of AISI 420 martensitic stainless steel using plasma nitriding at low temperature, Surface & Coatings Technology - SURF COAT TECH. 2008; 202: 2577–83.

[7] Liu W, Ma J, Atabaki M.M, Pillai R, Kumar B, Vasudevan U, et al. Hybrid Laser-arc Welding of 17-4 PH Martensitic Stainless Steel, Lasers in Manufacturing

and Materials Processing. 2015; 2(2): 74–90.
[8] Subodh Kumar A.S.S, Effect of heat input on the microstructure and mechanical properties of gas tungsten arc welded AISI 304 stainless steel joints, Materials and Design. 2011; 32(6): 3617–23.
[9] ASM handbook, welding, brazing and soldering. New york; 1993.
[10] Lippold J.C, Kotecki D.J, Welding metallurgy and weldability of stainless steels, Canada: John Wiley and Sons Inc. 2005.
[11] Dev S, Ramkumar K.D, Arivazhagan N, Rajendran R, Investigations on the microstructure and mechanical properties of dissimilar welds of inconel 718 and sulphur rich martensitic stainless steel, AISI 416. Journal of Manufacturing Processes. 2018; 32: 685–98.
[12] Fang J.X, Dong S.Y, Wang Y.J, Xu B.S, Zhang Z.H, Xia D, et al. Microstructure and properties of an as-deposited and heat treated martensitic stainless steel fabricated by direct laser deposition, Journal of Manufacturing Processes. 2017; 25: 402–10.
[13] Kou S, Welding Metallurgy, 2nd ed, New Jersey: John Wiley & Sons. 2003.
[14] Puli R, Ram G, Wear and corrosion performance of AISI 410 martensitic stainless steel coatings produced using friction surfacing and manual metal arc welding, Surface and Coatings Technology. 2012; 209: 1–7.
[15] Fam H, Kontopoulou M, Bryant J.T, Method for friction estimation in reciprocating wear tests, Wear. 2011; 271(5): 999–1003.
[16] Peruzzo M, Serafini F.L, Ordoñez M.F.C, Souza R.M, Farias M.C.M, Reciprocating sliding wear of the sintered 316L stainless steel with boron additions, Wear. 2019; 422–423: 108–18.
[17] Morón R.C, Rodríguez-Castro G,A, Melo-Máximo D.V, Oseguera J, Bahrami A, Muhl S, et al. Multipass and reciprocating microwear study of TiN based films, Surface and Coatings Technology. 2019; 375: 793–801.
[18] De Oliveira M.M, Costa H.L, Silva W.M, De Mello J.D.B, Effect of iron oxide debris on the reciprocating sliding wear of tool steels, Wear. 2019; 426–427: 1065–75.
[19] Archard J.F, Contact and Rubbing of Flat Surfaces, Journal of Applied Physics. 1953; 24(8): 981–8.
[20] Wang Y, Lei T, Liu J, Tribo-metallographic behavior of high carbon steels in dry sliding: II. Microstructure and wear, Wear. 1999; 231: 12–9.
[21] Krishnan S.N, Toppo V, Basak A, Ray K.K, Wear behaviour of a steel weld-joint, Wear. 2006; 260(11): 1285–94.
[22] Baghjari S.H, Malek Ghaini F, Previtali B, Gokhan Demir A, Shahverdi H.R, Mapelli C, et al. The effect of electrospark nickel interlayer thickness on the characteristics of Niobium to 410 stainless steel dissimilar laser welding, Journal of Manufacturing Processes. 2017; 30: 51–62.
[23] Pouranvari M, Sobhani S, Goodarzi F, Resistance spot welding of MS1200 martensitic advanced high strength steel: Microstructure-properties relationship, Journal of Manufacturing Processes. 2018; 31: 867–74.
[24] Hejripour F, Aidun D.K, Consumable selection for arc welding between Stainless Steel 410 and Inconel 718, Journal of Materials Processing Technology. 2017; 245: 287–99.
[25] Casalino G, Angelastro A, Perulli P, Casavola C, Moramarco V, Study on the fiber laser/TIG weldability of AISI 304 and AISI 410 dissimilar weld, Journal of Manufacturing Processes. 2018; 35: 216–25.
[26] Gouveia M.R, Silva J.G.F, Paiva C.O, Andrade F.M, Silva L, Moselli C.P, et al. Study of the Heat-Treatments Effect on High Strength Ductile Cast Iron Welded Joints, Metals. 2017; 7.
[27] Gouveia M.R, Silva J.G.F, Paiva C.O, De Fátima Andrade M, Pereira A.L, Moselli C.P, et al. Comparing the Structure and Mechanical Properties of Welds on Ductile Cast Iron (700 MPa) under Different Heat Treatment Conditions, Metals. 2018; 8.
[28] Marques S.V.E, Silva F.J.G, Paiva C.O, Pereira B.A, Improving the Mechanical Strength of Ductile Cast Iron Welded Joints Using Different Heat Treatments, Materials. 2019; 12.
[29] P. Suh N, The delamination theory of wear, Wear. 1973; 25(1): 111–24.